ACS Macro Letters

Letter

pubs.acs.org/macroletters

Manipulating Cellular Interactions of Poly(glycidyl methacrylate) Nanoparticles Using Mixed Polymer Brushes

Tristan D. Clemons,*[,†] Michael Challenor,[†,‡] Melinda Fitzgerald,[‡] Sarah A. Dunlop,[‡] Nicole M. Smith,[†,‡] and K. Swaminathan Iyer*[,†]

[†]School of Chemistry and Biochemistry and [‡]Experimental and Regenerative Neurosciences, School of Animal Biology, The University of Western Australia, 35 Stirling Hwy, Crawley, Western Australia 6009, Australia

Supporting Information

ABSTRACT: There is a growing need for the development of nanoparticles, with imaging and drug delivery capabilities, to maintain cellular uptake but avoid protein attachment and recognition. In this study we have demonstrated that nanoparticles consisting of a poly(glycidyl methacrylate) (PGMA) core and a mixed brush architecture of methoxypoly(ethylene glycol) and poly(ethylenimine) (mPEG−PEI) on the surface can meet this need. Surface functionalization with PEI alone results in cellular uptake, but rapid protein attachment whereas PEG alone can avoid protein attachment but to the detriment of cellular uptake. A mixed copolymer brush of both PEI and mPEG provides the ideal balance.

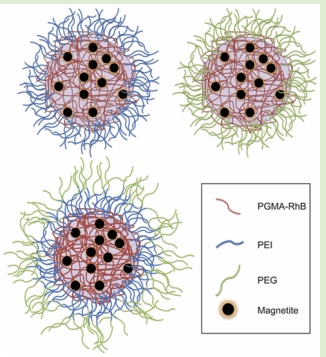

The application of nanoparticles for imaging and drug delivery is highly dependent on the ability to tailor the nanoparticle interactions with cells.[1] These interactions are pivotal in determining intracellular retention of the drugs and imaging agents within the target tissue. It is widely accepted that, compared to anionic or neutral nanoparticles, a cationic surface charge results in enhanced cell penetration owing to favorable interactions with the negatively charged cellular plasma membrane.[2] Furthermore, following intravenous administration, cationic nanoparticles are rapidly sequestered by the mononuclear phagocyte system (MPS) consisting of dendritic cells, blood monocytes, and tissue-resident macrophages in the liver, spleen, and lymph nodes, which are responsible for clearing these materials from circulation.[3] Clearance is in turn dependent on the adsorption of plasma proteins on the cationic nanoparticle surface.[4] This adsorption of proteins on the nanoparticle surface, often referred to as a protein corona, can significantly alter the biological identity of the nanoparticle and in turn can have dramatic effects on potential biomedical applications and toxicology.[5] The formation of the protein corona can be defined in the early phase as a "soft" corona with serum proteins loosely bound to the nanoparticle surface and in equilibrium with free surrounding serum proteins.[6] This soft corona can be easily displaced or stripped from the nanoparticle surface if the surrounding serum protein concentration was to decrease. This is in contrast to a "hard" protein corona where proteins lower in abundance but high in affinity for binding to the nanoparticle surface will begin to adsorb over time developing a persistent and more permanent protein coating.[6] This study will mainly focus on the acute interactions with proteins of three polymeric nanoparticles with modified surfaces and the effects this has on the nanoparticle cellular uptake. Proteins that bind to a nanoparticle surface act as opsonins that mark a nanoparticle for efficient uptake by the MPS and subsequent nanoparticle clearance.[3b,7] Previous studies have shown that adsorption of proteins onto the nanoparticle surface reduces the nanoparticle's ability to adhere to the cell membrane, resulting in reduced cellular uptake.[8] PEGylation of nanoparticle surfaces is commonly used to block protein adsorption.[9] The ability of PEG coatings to prevent protein adsorption is attributed to steric repulsion, resulting from loss of conformational freedom of PEG chains as they become compressed when the protein approaches the surface.[10] However, enhancement of circulation times using PEGylation also prevents active interaction and endocytosis in target cells.[11] In the present study using a "grafting to" approach to a colloidal poly(glycidyl methacrylate) (PGMA) nanoparticle core, we systematically demonstrate that while reducing protein adsorption on the nanoparticle surface it is possible to maintain active endocytosis of the nanoparticles using a mixed brush strategy incorporating both PEI and mPEG (Figure 1, and Supporting Information Figure S1).

The nanoparticles used in the current study consist of a rhodamine B-PGMA core (RhB-PGMA, see Supporting Information, Figure S1 for reaction scheme) containing encapsulated magnetite (Fe_3O_4) nanoparticles (Figure 2A) prepared from an oil in water emulsion process. The iron content of the nanoparticles was determined to be 2.5% w/w

Received: August 11, 2016
Accepted: September 19, 2016

DOI: 10.1021/acsmacrolett.6b00613
ACS Macro Lett. 2016, 5, 1132−1136

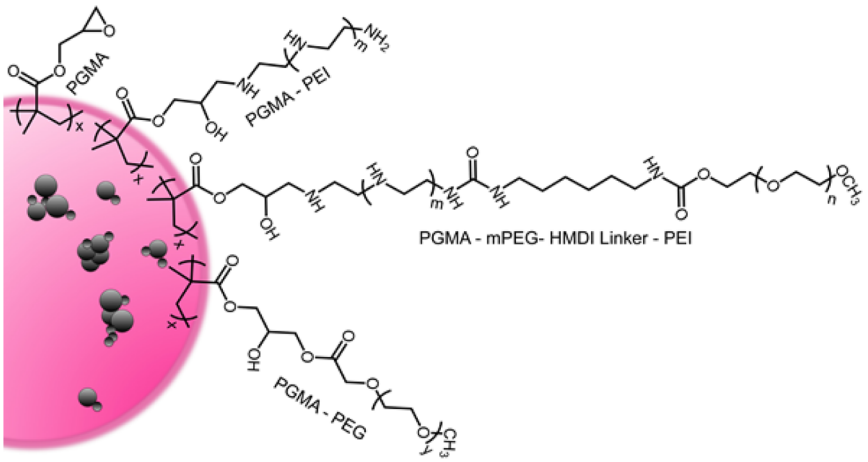

Figure 1. Schematic representation of the PGMA polymer nanoparticles and the surface modifications investigated for this study, PEI, mPEG–PEI, and PEG.

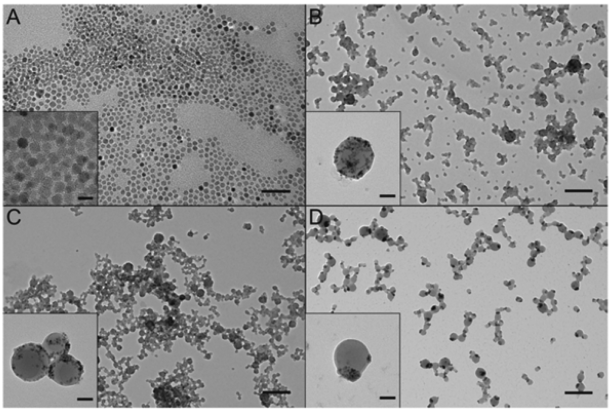

Figure 2. Transmission electron microscopy of (A) magnetite nanoparticles with high-magnification inset (scale 50 nm and inset 10 nm), (B) PEI-decorated PGMA nanoparticles with high-magnification inset, (C) PEG-decorated PGMA nanoparticles with high-magnification inset, and (D) mPEG–PEI-decorated PGMA nanoparticles with high-magnification inset. Scales for B–D are 500 nm with inset scale 50 nm.

by ICP-AES. RhB functionalization of the nanoparticles enabled tracking of the nanoparticle cellular interactions with fluorescence microscopy. The presence of Fe_3O_4 provides a means to separate, wash excess surfactant and reactants, as well as concentrate the nanoparticles using a magnetic fractionation column following surface modification of the PGMA core. Furthermore, Fe_3O_4 encapsulation also provides the potential for MRI contrast *in vivo* and cellular maneuverability of internalized nanoparticles with a magnetic field, which have been demonstrated in previous studies recently.[12] Both the fluorescent and magnetic capabilities of the nanoparticle cores have been demonstrated in culture, *ex vivo*, and *in vivo* studies previously.[12,13] Importantly, the glycidyl methacrylate units, located in the "loops" of the PGMA core and containing multiple free epoxy groups, serve as reactive sites for subsequent grafting of polymer chains. It has been demonstrated that increased mobility of the polymer chains in the PGMA core ensures better access to the epoxide functional groups, resulting in a 2- to 3-fold greater grafting density when compared with a monolayer of epoxy groups on a nanoparticle surface of similar dimension.[14] In the current study we analyzed grafting of short chain branched PEI, linear PEG, and mPEG–PEI (linear PEG with a branched PEI) copolymer to the PGMA-RhB core (see Supporting Information Figures S2–S4). PEI was chosen as a cationic polymer as it is the most widely used nonviral polymeric transfection agent.[15] However, despite efficient cellular uptake, these particles are also subject to rapid protein identification and in turn potential premature clearance via the MPS system.[3b]

The three nanoparticle systems used in this study were analyzed by dynamic light scattering (DLS) and found to have comparable hydrodynamic radii of approximately 150 nm (see Supporting Information, Figure S5 and Table S1), a finding supported by transmission electron microscopy (Figure 2). Despite identical solvent conditions during the emulsion process of each nanoparticle the distribution of the Fe_3O_4 is very different in all three systems. This suggests that polymer differences and the variability in the stability of the emulsion generated during sonication plays an important role in the Fe_3O_4 encapsulation. When analyzed in milli-Q water, the zeta potential of the nanoparticles was highest for PEI-decorated nanoparticles (52.9 mV), followed by mPEG–PEI-decorated (29.0 mV) and finally the PEG-decorated (−29.9 mV) nanoparticles (see Supporting Information, Figure S4 and Table S1). Nanoparticle samples were also assessed by DLS in the presence of both bovine serum albumin (BSA) and 10% human serum. In the presence of both BSA and human serum, all nanoparticle systems experienced an increase in hydrodynamic radii due to interactions with the serum proteins. Furthermore, all nanoparticles experienced a decrease in the absolute magnitude of the observed zeta potential (see Supporting Information, Table S1) in the presence of the serum proteins. These data taken together suggest an interaction between the serum proteins and all nanoparticle systems investigated in this study.

Cellular toxicity of these nanoparticle platforms was assessed *in vitro* using rat pheochromocytoma neural progenitor (PC12) cells. All three nanoparticle systems displayed no cellular toxicity *in vitro* up to a maximum concentration of 250 $\mu g\ mL^{-1}$ (see Supporting Information Figure S6). PEI alone has been shown to be cytotoxic, with the cellular toxicity increasing as the molecular weight of the PEI increases.[16] We have found that the short chain PEI used in this study for the PEI-decorated nanoparticles and others, combined with anchoring the PEI to the nanoparticle core, is able to alleviate the associated toxicity often seen with free PEI polymer chains.[17]

DOI: 10.1021/acsmacrolett.6b00613
ACS Macro Lett. 2016, 5, 1132–1136

Furthermore, previous studies have shown 25 kDa PEI to induce membrane damage and initiate apoptosis *in vitro*;[16b] however, this was not evident in our work with the mPEG–PEI-decorated nanoparticles. This again suggests that the anchoring to a nanoparticle substrate as well as the mPEG polymer coverage play a protective role with respect to cell toxicity. Confocal microscopy of PC12 cells following 24 h incubation with the nanoparticles was used to investigate the cellular uptake of each nanoparticle platform. Following washing to remove excess nanoparticles, images were collected from a single visual slice through the midsection of the cells to ensure nanoparticles present were truly intracellular. The PEI-decorated nanoparticles were readily internalized by cells, as expected and consistent with previous reports from our group (Figure 3A).[12b,13,17] Similarly the PEG-decorated PGMA

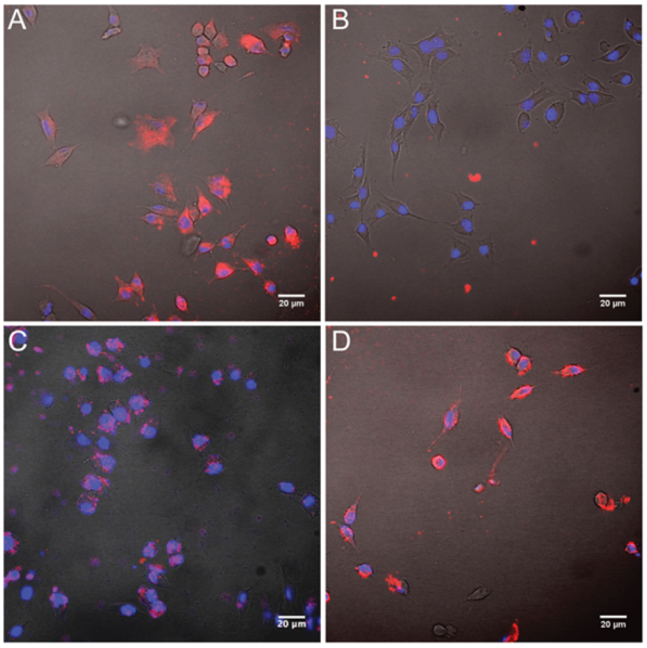

Figure 3. Confocal assessment of cellular uptake of nanoparticle preparations by PC12 cells following 24 h incubation: (A) PEI-coated nanoparticles, (B) PEG-coated nanoparticles, (C) mPEG–PEI-coated nanoparticles, all in growth medium, and (D) mPEG–PEI-decorated nanoparticles in the absence of serum in the media. All nanoparticle suspensions were at a final concentration of 20 μg mL^{-1}. All scale bars are 20 μm. All images are bright-field images with fluorescence from Rhodamine B labeled nanoparticles (red) and Hoechst stained nuclei (blue).

nanoparticle also behaved as expected, with no significant cellular association or uptake following the 24 h incubation period (Figure 3B). The mPEG–PEI-decorated nanoparticles showed similar results to that of the PEI nanoparticles, with strong cellular association and uptake regardless of the presence of serum in the incubation media (Figure 3C and 3D). Hence, despite the presence of serum proteins and the incorporation of the mPEG polymer on the nanoparticle surface, favorable cellular interactions can still be achieved with this mixed brush strategy.[2d]

Further to the assessment of cellular uptake in the neuronal culture conditions, cellular uptake in a phagocytic cell line was assessed in order to evaluate the effect of differing nanoparticle surfaces on phagocytosis. Nanoparticle uptake in ramified (nonactivated) microglia was compared to uptake by lipopolysaccharide (LPS) activated microglia (assessed via ED-1 immunoreactivity, see Supporting Information Figure S7). The addition of LPS to cell cultures has long been established as a method for activating microglia into a phagocytic inflammatory state.[18] Similar to the neuronal assessment, PEI-decorated nanoparticles were internalized by both activated and non-activated microglia (Figure 4A and B), and PEG-decorated

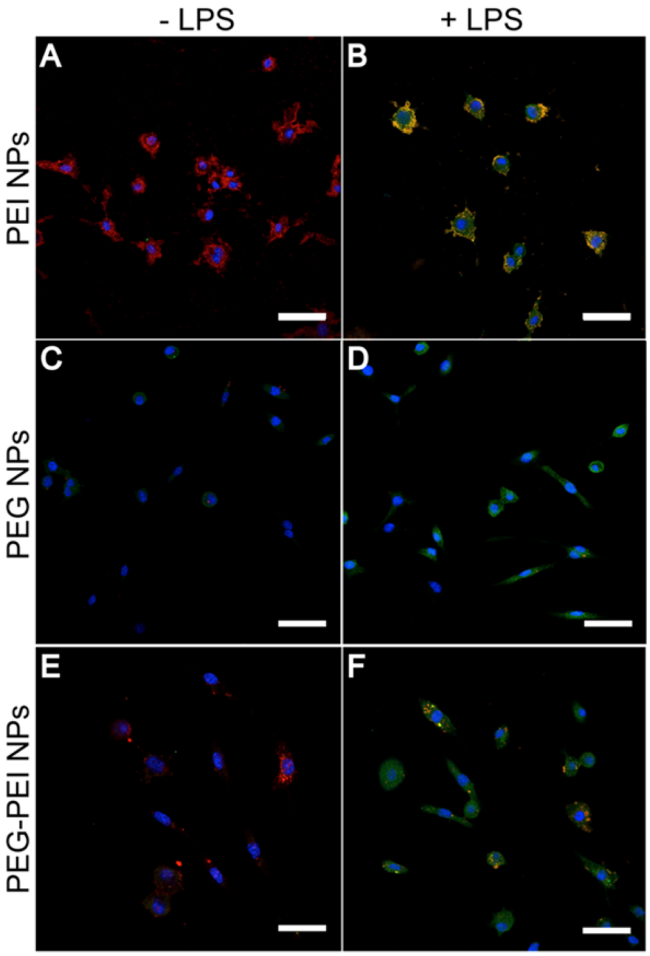

Figure 4. Confocal assessment of cellular uptake of nanoparticle preparations by LPS-activated and nonactivated microglia following 24 h incubation: (A) PEI-decorated nanoparticles, (B) PEI-decorated nanoparticles with LPS stimulation, (C) PEG-decorated nanoparticles, (D) PEG-decorated nanoparticles with LPS stimulation, (E) mPEG–PEI-decorated nanoparticles, and (F) mPEG–PEI-decorated nanoparticles with LPS stimulation. Nanoparticles labeled with Rhodamine B (red), ED-1 to assess microglial activation (green), and Hoechst (blue); all scale bars are 50 μm.

nanoparticles experienced effectively no cellular uptake by both activated and nonactivated microglia (Figure 4C and D). The mPEG–PEI-decorated nanoparticle uptake was again evident in both the activated and nonactivated microglia (Figure 4E and F).

Finally, to assess the nanoparticle's ability to avoid protein adsorption and mimic opsonin identification in the body, nanoparticles were incubated with bovine serum albumin (BSA) to assess the degree of protein binding. BSA is an ideal model protein for this experiment, as it is a common and abundant globular serum protein with many similar characteristics to that of human serum albumin and its potential binding

DOI: 10.1021/acsmacrolett.6b00613
ACS Macro Lett. 2016, 5, 1132–1136

with nanoparticles.[19] It was found that the highly cationic PEI-coated nanoparticles significantly bound a large proportion of the BSA present (Figure 5), leading to nanoparticle instability

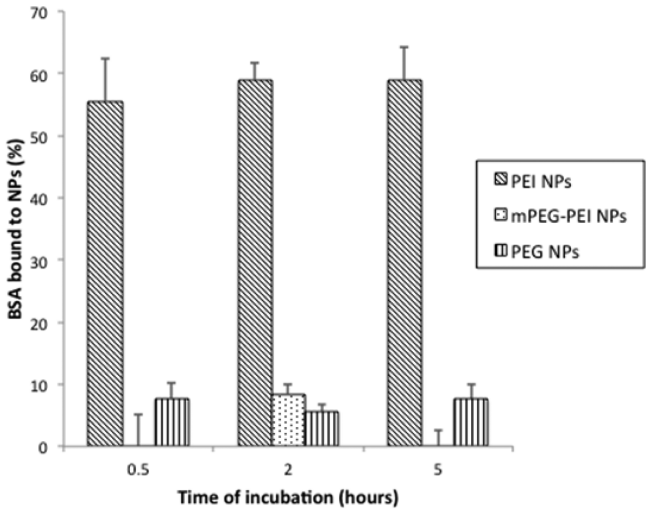

Figure 5. Time course assessment of bovine serum albumin (BSA) binding to the PEI, PEG, or mPEG–PEI-decorated nanoparticles. Data displayed as mean ± standard error of n = 3 measurements.

and aggregation within 30 min. As expected, the PEGylated nanoparticles were able to avoid protein binding across all time points out to 5 h. The mPEG–PEI copolymer decorated nanoparticles were also able to avoid aggregation and significant BSA adsorption across the 5 h time frame. For the mPEG–PEI-decorated nanoparticles the percentage of bound BSA on the nanoparticles was 5.4%, 1.5%, and 3.6% at 0.5 h, 2 h, and 5 h, respectively. Taken together, our data suggest that a mPEG–PEI nanoparticle platform is able to achieve cellular uptake while also avoiding ubiquitous protein adsorption. Together these results provide promise for a nanoparticle platform suitable for intracellular delivery of therapeutics while being able to avoid premature protein recognition and clearance.

In summary, we have demonstrated that through systematic modification of a PGMA core with a mixed polymer brush surface architecture we can achieve both cellular uptake of the nanoparticle while minimizing protein interaction on the nanoparticle surface. This is an important finding for the development and use of similar polymeric nanoparticles for biological applications.

EXPERIMENTAL SECTION

Nanoparticle Synthesis and Characterization. All nanoparticles were synthesized making use of an emulsion synthesis protocol described previously and detailed in full in the Supporting Information.[17] FTIR analysis of the mPEG–PEI copolymer was performed on a PerkinElmer Spectrum One FT-IR Spectrometer. FTIR analysis clearly shows the expected absence of C–O ether stretching in the PEI and the absence of amine and cyano stretches in the mPEG sample, but clearly shows the combination of these signals in the copolymer with the evolution of the C=O stretch (1660 cm^{-1}) formed during the linking process (see Supporting Information, Figure S1). ^{1}H NMR (500 MHz) and ^{13}C NMR (125 MHz) spectra of the copolymer were recorded on a Bruker AV500 instrument in 5 mm NMR tubes. Samples were recorded in D_2O solution in parts per million and referenced to the internal D_2O singlet at 4.79 ppm. ^{13}C and ^{1}H NMR analysis of the copolymer revealed successful linking of mPEG and PEI with a hexamethylene diisocyanate (HMDI) linker (see Supporting Information, Figure S2). Dynamic light-scattering (DLS) measurements of size and zeta potential of nanoparticle preparations were performed on a Malvern Zetasizer instrument on nanoparticle samples suspended in milli-Q water, in the presence of 0.5 mg mL^{-1} of BSA or in the presence of 10% human serum. Samples prepared for transmission electron microscopy analysis were prepared by depositing onto carbon-coated grids and imaged at 120 kV on a JEOL JEM-2100. The iron content of the PGMA nanoparticles was determined by ICP-AES after acid digestion (5 mL).

Cell Culture. PC12 neuronal cells were maintained in RPMI1640 medium containing horse serum (10%), fetal bovine serum (5%), penicillin/streptomycin (100 U mL^{-1}, 100 μg mL^{-1}), L-glutamine (2 mM), nonessential amino acids (100 μM), and sodium pyruvate (1 mM) (referred to as growth medium) and were incubated in a humidified atmosphere containing 5% CO_2 at 37 °C. For experiments, cells were either seeded on 10 mm coverslips for confocal assessment or 96-well plates for cellular viability assessments. All culture surfaces were coated with 0.1 mg mL^{-1} poly(L-lysine) (Sigma), and cells were plated at a cell density of 0.5–1 × 10^5 cells mL^{-1}. Cells were not differentiated with NGF. EOC2 CRL-2467 microglial cells were maintained in Dulbecco's modified Eagle's medium with 4 mM L^{-1} glutamine adjusted to contain 1.5 g L^{-1} sodium bicarbonate and 4.5 g L^{-1} glucose, 70%; fetal bovine serum, 10%; and LADMAC Conditioned Media (produced from the LADMAC cell line (CRL-2420), 20%. Cells were incubated in a humidified atmosphere containing 5% CO_2 at 37 °C.

Cell Viability PC12 Neuronal Cells. Viability was measured using a Live/Dead cell kit (Invitrogen). PC12 cells were seeded at 1 × 10^5 cells mL^{-1} in growth media and preincubated for 24 h before the media was replaced with nanoparticle suspensions of different concentrations in growth media (n = 3 minimum). Cells were incubated with nanoparticles for 24 h and then washed with PBS and incubated for 30 min with 100 μL of the detection reagents (Calcein AM, 1 μM; ethidium homodimer-1, 2–3 μM). Images were recorded using an inverted fluorescence microscope at 20× magnification (Olympus IX-71, Olympus IX-81). Four images were recorded from each well at consistent locations for all wells and all experiments, and live and dead cells were counted.

Confocal Analysis. PC12 neuronal cells were grown on coverslips as described above and incubated with nanoparticles in growth media at 20 μg mL^{-1} for 24 h before being washed with PBS and fixed in 4% paraformaldehyde (Sigma). Cell nuclei were visualized using Hoechst 33342 (Sigma, 1 μg mL^{-1}) following standard protocols. Images were captured by confocal microscopy (Leica TCS SP2, Nikon A1Si). RhB was detected with a laser excitation of 516 nm and an emission collection window of 570–620 nm. Hoechst was detected with the Spectra-physics Mai-Tai multiphoton laser, pulsed, and centered at 800 nm with a detection collection window of 400–450 nm. EOC2 CRL-2467 microglial cells were plated on Lab-Tek 8-well chamber slides at a concentration of 1250 cells/well. Cells were left overnight to adhere before growth media was replaced with either fresh growth media (nonstimulating) or with growth media supplemented with 100 ng mL^{-1} LPS (stimulating media) before a further 24 h incubation. Control and nanoparticle solutions (control (no nanoparticles), PEI-decorated, PEG-decorated, and mPEG–PEI-decorated nanoparticles) were prepared in either control growth media or in the LPS-stimulating media at a final nanoparticle concentration of 20 μg mL^{-1}. Following the LPS stimulation (24 h) media was removed from all wells; nanoparticle solutions in growth media were added to nonstimulated cells; and nanoparticles in stimulating media were added to stimulated cells. Following 24 h of nanoparticle incubation, media was removed, and cells were washed with PBS and fixed in 4% paraformaldehyde (Sigma). Immunohistochemistry for ED1 expression, 1:500 dilution anti-CD68 [ED1] (Abcam, ab31630) primary, visualized with Alexa Fluor 488 secondary (ThermoFisher a21202) and cell nuclei were visualized using Hoechst 33342 (Sigma, 1 μg mL^{-1}), following standard protocols. Images were captured by confocal microscopy on a Nikon Ti-E inverted motorized microscope with a Nikon A1Si spectral detector confocal system running NIS-C Elements software. All samples were conducted in duplicate and n = 5 images as minimum collected per treatment.

DOI: 10.1021/acsmacrolett.6b00613
ACS Macro Lett. 2016, 5, 1132–1136

Protein Attachment Experiment. Triplicate samples were prepared containing 100 μg of nanoparticles (PEI, PEG, mPEG–PEI-decorated nanoparticles) with 50 μg of BSA in a total volume of 100 μL of milli-Q H_2O. Control preparations did not contain nanoparticles. Samples were incubated for either 0.5, 2, or 5 h before centrifugation (14 000 rpm, 30 min) to remove nanoparticles and bound BSA. Aliquots of the supernatant were collected and measured for absorbance on a Nanodrop UV–vis instrument where the absorbance was compared to a prepared BSA standard curve (see Supporting Information, Figure S8 for the standard curve). Concentration of the BSA in supernatants was calculated and percentage of BSA bound to nanoparticles determined.

■ ASSOCIATED CONTENT

Supporting Information

The Supporting Information is available free of charge on the ACS Publications website at DOI: 10.1021/acsmacrolett.6b00613.

Complete synthesis protocols for the nanoparticles used in this study as well as supporting experiments including FTIR and NMR characterization of the PEG–PEI copolymer and cellular toxicity studies with the nanoparticles (PDF)

■ AUTHOR INFORMATION

Corresponding Authors

*E-mail: tristan.clemons@uwa.edu.au.
*E-mail: swaminatha.iyer@uwa.edu.au.

Notes

The authors declare no competing financial interest.

■ ACKNOWLEDGMENTS

The authors would like to acknowledge Ms Naina Akella, for her work on this project as a part of the WA state government run BioGENEius challenge. The authors also acknowledge the Australian Microscopy & Microanalysis Research Facility at the Centre for Microscopy, Characterization & Analysis, The University of Western Australia, funded by the University, State and Commonwealth Governments. This work was funded by the Australian Research Council (ARC), the National Health & Medical Research Council (NHMRC) of Australia, and the Raine Medical Research Foundation. Tristan Clemons is a NHMRC Peter Doherty – Australian Biomedical Fellow; Melinda Fitzgerald is a NHMRC Career Development Fellow; and K. Swaminathan Iyer is an ARC Future fellow.

■ REFERENCES

(1) Mailander, V.; Landfester, K. *Biomacromolecules* **2009**, *10* (9), 2379–2400.

(2) (a) Frohlich, E. *Int. J. Nanomed.* **2012**, *7*, 5577–5591. (b) Nafee, N.; Schneider, M.; Schaefer, U. F.; Lehr, C. M. *Int. J. Pharm.* **2009**, *381* (2), 130–139. (c) Shenoy, D. B.; Amiji, M. A. *Int. J. Pharm.* **2005**, *293* (1–2), 261–270. (d) Verma, A.; Stellacci, F. *Small* **2010**, *6* (1), 12–21.

(3) (a) Kumari, A.; Yadav, S. K.; Yadav, S. C. *Colloids Surf., B* **2010**, *75* (1), 1–18. (b) Song, G.; Petschauer, J. S.; Madden, A. J.; Zamboni, W. C. *Curr. Rheumatol. Rev.* **2014**, *10* (1), 22–34.

(4) (a) Liu, F.; Liu, D. X. *Biochim. Biophys. Acta, Biomembr.* **1996**, *1278* (1), 5–11. (b) Patil, S.; Sandberg, A.; Heckert, E.; Self, W.; Seal, S. *Biomaterials* **2007**, *28* (31), 4600–4607.

(5) (a) Casals, E.; Pfaller, T.; Duschl, A.; Oostingh, G. J.; Puntes, V. *ACS Nano* **2010**, *4* (7), 3623–3632. (b) Tenzer, S.; Docter, D.; Kuharev, J.; Musyanovych, A.; Fetz, V.; Hecht, R.; Schlenk, F.; Fischer, D.; Kiouptsi, K.; Reinhardt, C.; Landfester, K.; Schild, H.; Maskos, M.; Knauer, S. K.; Stauber, R. H. *Nat. Nanotechnol.* **2013**, *8* (10), 772–U1000.

(6) Foroozandeh, P.; Aziz, A. A. *Nanoscale Res. Lett.* **2015**, DOI: 10.1186/s11671-015-0922-3.

(7) Frank, M. M.; Fries, L. F. *Immunol. Today* **1991**, *12* (9), 322–6.

(8) Lesniak, A.; Salvati, A.; Santos-Martinez, M. J.; Radomski, M. W.; Dawson, K. A.; Aberg, C. *J. Am. Chem. Soc.* **2013**, *135* (4), 1438–1444.

(9) (a) Li, S. D.; Huang, L. *J. Controlled Release* **2010**, *145* (3), 178–181. (b) Niidome, T.; Yamagata, M.; Okamoto, Y.; Akiyama, Y.; Takahashi, H.; Kawano, T.; Katayama, Y.; Niidome, Y. *J. Controlled Release* **2006**, *114* (3), 343–347. (c) Perry, J. L.; Reuter, K. G.; Kai, M. P.; Herlihy, K. P.; Jones, S. W.; Luft, J. C.; Napier, M.; Bear, J. E.; DeSimone, J. M. *Nano Lett.* **2012**, *12* (10), 5304–5310.

(10) Bazile, D.; Prud'homme, C.; Bassoullet, M. T.; Marlard, M.; Spenlehauer, G.; Veillard, M. *J. Pharm. Sci.* **1995**, *84* (4), 493–8.

(11) Gref, R.; Minamitake, Y.; Peracchia, M. T.; Trubetskoy, V.; Torchilin, V.; Langer, R. *Science* **1994**, *263* (5153), 1600–3.

(12) (a) Bradshaw, M.; Clemons, T. D.; Ho, D.; Gutierrez, L.; Lazaro, F. J.; House, M. J.; Pierre, T. G. S.; Fear, M. W.; Wood, F. M.; Iyer, S. *Nanoscale* **2015**, *7* (11), 4884–4889. (b) Tangudu, N. K.; Verma, V. K.; Clemons, T. D.; Beevi, S. S.; Hay, T.; Mahidhara, G.; Raja, M.; Nair, R. A.; Alexander, L. E.; Patel, A. B.; Jose, J.; Smith, N. M.; Zdyrko, B.; Bourdoncle, A.; Luzinov, I.; Iyer, K. S.; Clarke, A. R.; Dinesh Kumar, L. *Mol. Cancer Ther.* **2015**, *14* (5), 1259–69.

(13) Clemons, T. D.; Viola, H. M.; House, M. J.; Iyer, K. S.; Hool, L. C. *ACS Nano* **2013**, *7* (3), 2212–2220.

(14) Iyer, K. S.; Zdyrko, B.; Malz, H.; Pionteck, J.; Luzinov, I. *Macromolecules* **2003**, *36* (17), 6519–6526.

(15) (a) Akinc, A.; Thomas, M.; Klibanov, A. M.; Langer, R. *J. Gene Med.* **2005**, *7* (5), 657–663. (b) Al-Dosari, M. S.; Gao, X. *AAPS J.* **2009**, *11* (4), 671–681.

(16) (a) Hunter, A. C. *Adv. Drug Delivery Rev.* **2006**, *58* (14), 1523–1531. (b) Moghimi, S. M.; Symonds, P.; Murray, J. C.; Hunter, A. C.; Debska, G.; Szewczyk, A. *Mol. Ther.* **2005**, *11* (6), 990–995.

(17) Evans, C. W.; Fitzgerald, M.; Clemons, T. D.; House, M. J.; Padman, B. S.; Shaw, J. A.; Saunders, M.; Harvey, A. R.; Zdyrko, B.; Luzinov, I.; Silva, G. A.; Dunlop, S. A.; Iyer, K. S. *ACS Nano* **2011**, *5* (11), 8640–8648.

(18) (a) Hughes, M. M.; Field, R. H.; Perry, V. H.; Murray, C. L.; Cunningham, C. *Glia* **2010**, *58* (16), 2017–2030. (b) Stansley, B.; Post, J.; Hensley, K. *J. Neuroinflammation* **2012**, DOI: 10.1186/1742-2094-9-115. (c) Taylor, D. L.; Diemel, L. T.; Pocock, J. M. *J. Neurosci.* **2003**, *23* (6), 2150–2160.

(19) Boulos, S. P.; Davis, T. A.; Yang, J. A.; Lohse, S. E.; Alkilany, A. M.; Holland, L. A.; Murphy, C. J. *Langmuir* **2013**, *29* (48), 14984–14996.

DOI: 10.1021/acsmacrolett.6b00613
ACS Macro Lett. 2016, 5, 1132–1136